

Charge transfer and association of Na^+ with ^{87}Rb atoms from extremely low to intermediate energies

L. L. Yan,¹ L. Liu,¹ Y. Wu,¹ Y. Z. Qu,² J. G. Wang,¹ and R. J. Buenker³¹*Data Center for High Energy Density Physics, Institute of Applied Physics and Computational Mathematics, PO Box 8009, Beijing 100088, China*²*College of Material Sciences and Optoelectronic Technology, University of the Chinese Academy of Sciences, PO Box 4588, Beijing 100049, China*³*Fachbereich C-Mathematik und Naturwissenschaften, Bergische Universität Wuppertal, D-42097 Wuppertal, Germany*

(Received 15 May 2013; published 18 July 2013)

The nonradiative charge-transfer processes in $\text{Na}^+ + ^{87}\text{Rb}(5s)$ collisions have been investigated by using the quantum-mechanical molecular-orbital close-coupling method and the two-center atomic-orbital close-coupling method for the energy range of 10^{-4} –5 and 0.3–100 keV/u, respectively. The radiative charge-transfer, radiative-decay, and radiative-association processes have been investigated by using the fully quantum, optical-potential, and semiclassical methods for the energy range of 10^{-18} –0.2 eV/u. The nonradiative charge-transfer processes dominate the collisions for energies above 0.2 eV/u and radiative-decay processes dominate in the lower-energy region. At the very low collision energies of 10^{-18} – 10^{-3} eV/u, the radiative-association process is more important than the radiative charge-transfer process. Most importantly, it is found that the radiative cross sections exhibit Langevin behavior as $E^{-1/2}$ for energies less than 10^{-2} eV/u.

DOI: [10.1103/PhysRevA.88.012709](https://doi.org/10.1103/PhysRevA.88.012709)

PACS number(s): 34.70.+e, 34.20.-b

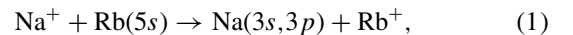
I. INTRODUCTION

Alkali-metal ion-atom collisions at cold temperatures have received considerable attention because of their importance in the cooling and trapping of atoms and molecules and in the investigations of cold plasmas [1–3]. Since the magneto-optical traps have been developed, trap loss in the form of molecular ions has been observed [4]. The populations of alkali-metal atoms and ions and their emission spectra are significantly influenced by charge-transfer or association processes in the collisions. These characteristic spectra are important for studying the charge transport and diagnosing the density of laboratory cold plasmas.

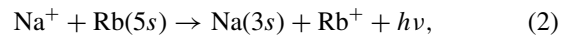
A number of studies aimed at understanding these dynamical processes for Na^+ colliding with $\text{Rb}(5s)$ atoms have been performed. Lee *et al.* [2] have measured single-electron capture differential cross sections for collision energies at 2, 5, and 7 keV by using magneto-optical trap-target recoil ion momentum spectroscopy (MOTRIMS). The ratio between the capture cross sections to $\text{Na}(3s)$ and $\text{Na}(3p)$ was inferred from the measurements. Later, Blicek *et al.* [3] developed the MOTRIMS apparatus and measured the differential cross sections with a low-background level for Na^+ colliding with trapped ^{87}Rb atoms at 2 keV. Lee *et al.* [2] and Lin *et al.* [5] have calculated the cross sections using an atomic-orbital close-coupling (AOCC) method for collisions at 2, 5, and 7 keV. These earlier works focused mainly on the energy region of several keV where the direct charge transfer dominates. As is well known, the cooling of neutral atoms and atomic ions with the currently available technology of laser cooling is possible down to the submillikelvin temperature regime, and forms cold molecular ions by atom-ion cold collisions [6,7]. The radiative-decay (including radiative charge transfer and radiative association) process may become dominant in the energy region. Usually, the radiative decay is a process with much lower probability because the time needed to emit the photon from the excited state ($\sim 10^{-8}$ s) is much longer and the typical cross section (five orders of or smaller than the elastic

scattering cross section) is much smaller. There are cases, however, where the formation of bound, excited molecular ions can make a contribution to the observed spectra, and the radiative process is a possible mechanism to explain the experimental findings [6]. Especially when the final state has a deep potential well, the contribution from radiative association to total radiative decay is important and this could result in a large radiative-association cross section, which could provide an efficient way to produce cold ions through collisions with neutral gas. Furthermore, there exist many disputations about the range of applicability for the Langevin formula [8,9]. Schuessler *et al.* [10] have verified energy dependence $E^{-1/2}$ of the charge-transfer cross section for collisions of He^+ with Cs atoms at energies from 0.1 to 1 eV by experiment. Hadjar *et al.* [11] have observed the Langevin-type ion-atom collisions of Ne^{2+} with Ne atoms in the energy range from 0.3 to 10 eV. However, they both deal with the direct charge-transfer cross sections, whereas investigations of radiative decay in the extremely low energy (cold) region are sparse.

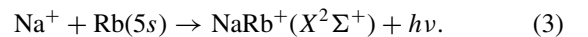
In the present work, we shall study the collisions of Na^+ with $^{87}\text{Rb}(5s)$ atoms in the energy region from 10^{-18} eV/u to 100 keV/u. Several processes are investigated, namely, the nonradiative charge-transfer process,



radiative charge-transfer process,



and radiative-association process,



The nonradiative charge-transfer cross sections are calculated by using the full quantum-mechanical molecular-orbital close-coupling (QMOCC) method in the energy range of 10^{-4} –5 keV/u and by the two-center atomic-orbital close-coupling (TC-AOCC) method in the energy range of 0.3–100 keV/u. The radiative-decay cross sections are calculated by using

TABLE I. Asymptotic separated-atom energies for the states of NaRb⁺.

Asymptotic atomic states	Molecular states	Energy (cm ⁻¹)		
		NIST [17]	MRD-CI	Error
Na(3s ² S) + Rb ⁺ (4p ⁶)	1 ² Σ ⁺	-7759	-7758	1
Na ⁺ + Rb(5s ² S)	2 ² Σ ⁺	0	0	0
Na(3p ² P) + Rb ⁺ (4p ⁶)	3 ² Σ ⁺	9206	9212	6
Na(3p ² P) + Rb ⁺ (4p ⁶)	1 ² Π	9206	9212	6
Na ⁺ + Rb(5p ² P)	4 ² Σ ⁺	12698	12703	5
Na ⁺ + Rb(5p ² P)	2 ² Π	12698	12703	5

the optical-potential and semiclassical method, respectively, for the energy range of 10^{-18} –0.2 eV/u. The radiative charge-transfer cross sections are calculated by using the fully quantum method for the energy range of 10^{-18} – 3×10^{-3} eV/u. The radiative-association cross sections are obtained by subtracting the radiative charge-transfer part from total radiative-decay cross sections. The molecular structure data (potential curves, radial and rotational couplings, and dipole transition matrix elements) required in the scattering calculations have been calculated using the *ab initio* multireference single- and double-excitation configuration interaction (MRD-CI) method.

The rest of the paper is organized as follows. Section II describes the molecular potential and coupling data utilized in the scattering calculations, while Sec. III discusses the scattering calculation approach. Section IV presents the results of the scattering calculation. A brief summary is given in Sec. V. Atomic units are used throughout unless otherwise noted.

II. ELECTRONIC STRUCTURE CALCULATIONS

In the present study, *ab initio* multireference configuration interaction calculations are carried out for adiabatic potential energies of four ²Σ⁺ states in A₁ (C_{2v}) symmetry and two ²Π states in B₁ symmetry of the NaRb⁺ system by employing the MRD-CI package [12,13]. For the sodium and rubidium atoms, effective core potentials (ECP) [14,15] are used to describe the corresponding inner-shell electrons. The remaining (highest) inner-shell (2s and 2p for Na, 4s and 4p for Rb) and valence electrons (3s for Na, 5s for Rb) are considered explicitly in the *ab initio* self-consistent field (SCF) and CI calculations. The ECP-adapted (6s, 4p) and (5s, 5p) Gaussian basis sets and the added diffuse basis (1s, 2p, 2d, 1f) and (1s, 1p, 4d, 2f) are utilized to describe the highest inner-shell electrons and the valence electrons of the Na and Rb atoms, respectively. The linear dependency in the basis set for the short internuclear distance region has been checked. The correlation coefficients are smaller than 10^{-4} and there are no serious linear correlations. A threshold of 2×10^{-10} Hartree is applied in the selection of the configuration wave functions. The errors in the asymptotic energies of the relevant electronic states are given in Table I. Good agreement is obtained with the present theoretical results and the experimental measurements. The obtained electronic wave functions are then employed to calculate radial and rotational couplings by using finite differentiation and analytical approaches, respectively [16].

In Fig. 1, the calculated adiabatic potential energy curves for the lowest four ²Σ⁺ and two ²Π molecular states are presented as a function of internuclear distance, where the 2 ²Σ⁺ state represents the initial channel in Na⁺ + Rb(5s) collisions. A relatively strong avoided crossing exists at about 5.0 a.u. between 3 ²Σ⁺ and 4 ²Σ⁺ states. For an internuclear distance less than 10 a.u., the potential curves of the 1 ²Π state and the 2 ²Σ⁺ state approach each other quickly with decreasing of R, and the rotational coupling between them becomes somewhat important.

In Table II, the present calculated spectroscopic constants, including equilibrium positions R_e and depths of potential wells D_e , are compared with the available theoretical calculations [18,19]. It can be observed that the depth of the potential well of the ground state by Valance [18] is much smaller than the present result as well as the one of Bellomonte *et al.* [19], which is possibly due to the fact that the linear combination of atomic orbitals (-molecular orbitals) (LCAO-MO) trial wave function applied in Valance's calculation [18] is not sufficiently accurate. The present potential wells are found to be much deeper than the one-active-electron calculations by Valance [18]. The reason for the above discrepancies is that in our *ab initio* multielectron calculations, a close encounter and interaction in the region of molecular coupling will lead to the

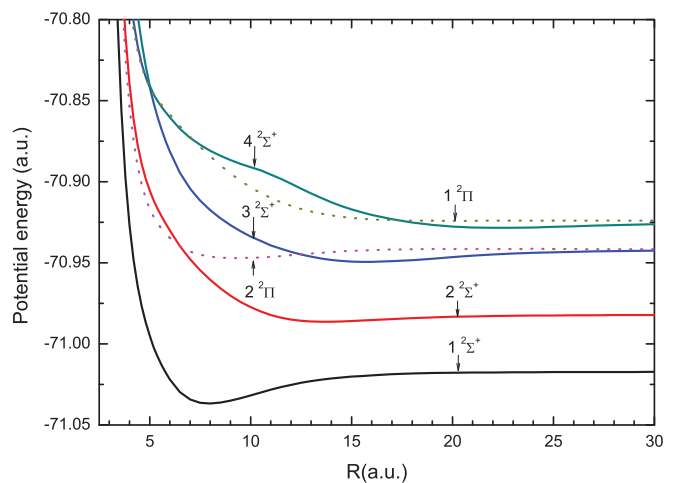


FIG. 1. (Color online) Adiabatic potential curves for NaRb⁺ as a function of internuclear distance. Solid lines denote the ²Σ⁺ states; dotted lines the ²Π states. The 1 ²Σ⁺, 2 ²Σ⁺, 3 ²Σ⁺, 4 ²Σ⁺, 1 ²Π, and 2 ²Π states correspond to the Na(3s) + Rb⁺, Na⁺ + Rb(5s), Na(3p) + Rb⁺, Na⁺ + Rb(5p), Na(3p) + Rb⁺, and Na⁺ + Rb(5p) channels in the asymptotic region, respectively.

TABLE II. Equilibrium positions R_e (a.u.) and depths D_e (eV) of potential wells for the $2\Sigma^+$ and 2Π states of NaRb⁺.

Molecular states	Present		Valance [18]		Bellomonte [19]	
	R_e	D_e	R_e	D_e	R_e	D_e
$1\ 2\Sigma^+$	8.0	0.531	8.0	0.310	7.5	0.60
$2\ 2\Sigma^+$	13.5	0.132	14.0	0.094		
$3\ 2\Sigma^+$	16.0	0.215	17.0	0.066		
$4\ 2\Sigma^+$	22.0	0.124	22.0	0.038		
$1\ 2\Pi$	9.5	0.150				

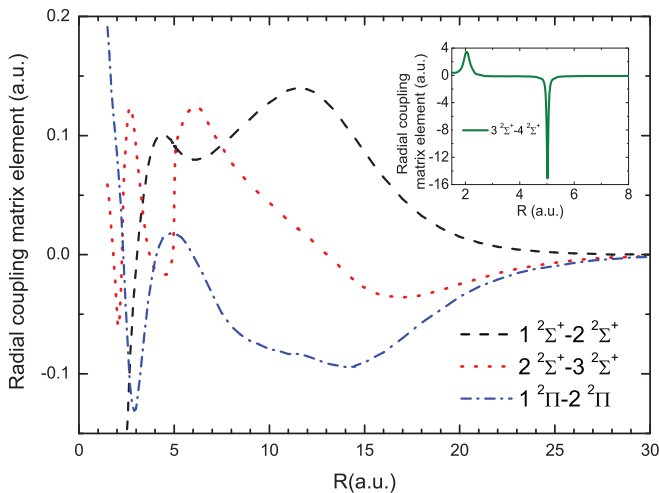
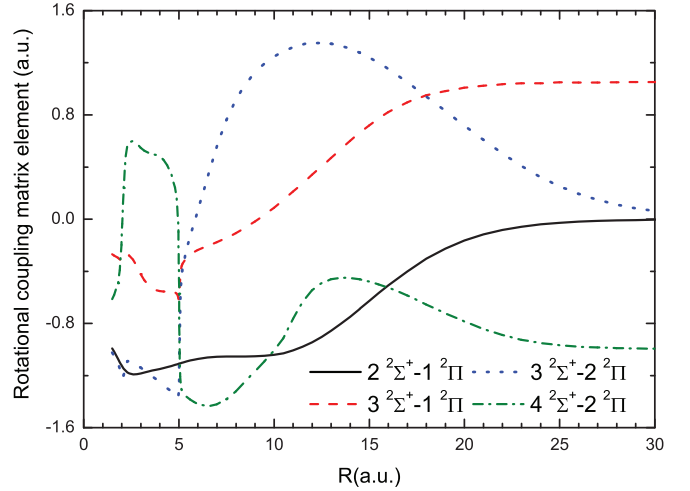
electronic excitation out of an inner shell, which indicates that one-active-electron calculations are not reliable in the critical small- R region [20].

In Fig. 2, the radial coupling matrix elements are presented as a function of internuclear distance, which have been calculated by finite difference approximation,

$$A_{ij}^R = \langle \psi_i | \frac{\partial}{\partial R} | \psi_j \rangle = \lim_{\Delta R \rightarrow 0} \frac{1}{\Delta R} \langle \psi_i(R) | \psi_j(R + \Delta R) \rangle, \quad (4)$$

with the step size of 0.0005 a.u. It is evident that the positions of the peaks in radial couplings are consistent with the avoided crossings of the adiabatic potentials, as shown in Fig. 1. It can be seen that the initial channel of $2\ 2\Sigma^+$ state is coupled with the $1\ 2\Sigma^+$ state at internuclear distance about 11.5 a.u., which drives the electronic transition to the Na($3s$) + Rb⁺ state at low collision energies. There are two maxima in the $2\ 2\Sigma^+ - 3\ 2\Sigma^+$ coupling at the internuclear separations of about 2.7 and 6.0 a.u., and this coupling plays an important role in high-energy collisions. A very sharp peak is observed near $R = 5.0$ a.u. for the $3\ 2\Sigma^+ - 4\ 2\Sigma^+$ coupling. The $4\ 2\Sigma^+$ channel will play an important role in collision-excitation processes at high energies, which are not considered in the present study.

In Fig. 3, some important rotational coupling matrix elements of $A_{ij}^\theta = \langle \psi_i | L_y | \psi_j \rangle$ are presented as a function of internuclear distance. The rotational couplings approach zero at a large internuclear distance for the two states belonging to different configurations, such as the $2\ 2\Sigma^+ - 1\ 2\Pi$ coupling.

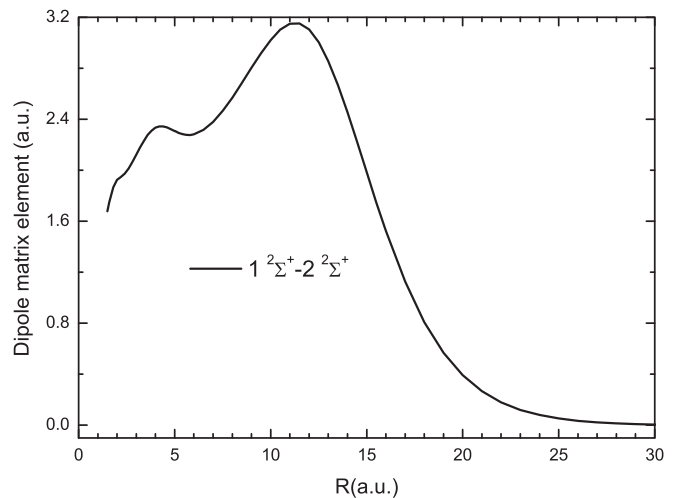
FIG. 2. (Color online) Radial coupling matrix elements for NaRb⁺.FIG. 3. (Color online) Rotational coupling matrix elements for NaRb⁺.

Otherwise, the couplings will approach a constant value if the two states belong to the same configuration, such as the $3\ 2\Sigma^+ - 1\ 2\Pi$ coupling. Note that the $2\ 2\Sigma^+ - 1\ 2\Pi$ coupling plays a significant role in electron capture to the Na($3p$) + Rb⁺ channel. In Fig. 4, the dipole transition moment between the $1\ 2\Sigma^+$ and $2\ 2\Sigma^+$ states is presented, and a broad maximum can be observed for R at about 11.5 a.u., which corresponds to the position of the avoided crossing between the two states. The dipole transition moment is responsible for the radiative-decay processes in the collisions.

III. SCATTERING CALCULATIONS

A. QMOCC method for nonradiative charge transfer

The QMOCC method used to describe the nonradiative charge transfer in ion-atom collisions has been formulated by Zygelman and Dalgarno [21] and Kimura and Lane [22], and here we only outline it briefly. It involves solving a coupled set of second-order differential equations using the log-derivative method [23]. In the adiabatic representation, transitions between channels are driven by elements

FIG. 4. Dipole matrix element for NaRb⁺.

(radial A^R and rotational A^θ) of the vector potential $A(\vec{R})$, where \vec{R} is the internuclear distance vector. Since the adiabatic description contains first-order derivatives, it is numerically convenient to make a unitary transformation [21,24] to a diabatic representation,

$$U(R) = W(R)[V(R) - P(R)]W^{-1}(R), \quad (5)$$

where $U(R)$ is the diabatic potential matrix, $V(R)$ is the diagonal adiabatic potential, $W(R)$ is a unitary transformation matrix, and $P(R)$ is the rotational matrix of the vector potential $A(\vec{R})$.

The coupled set of second-order differential equations is solved by employing the diabatic potentials and couplings. The charge-capture cross section from initial channel i to the final channel j is given by

$$\sigma_{(i \rightarrow j)} = \frac{\pi}{k_i^2} \sum_J (2J+1) |S_J|_{i,j}^2, \quad (6)$$

where k_i is the initial momentum, J is the total angular momentum, and scattering matrix S is

$$S_J = [I + iK_J]^{-1}[I - iK_J], \quad (7)$$

where I is the identity matrix, and the K matrix is obtained from the scattering amplitude after a partial-wave decomposition [21]. We have not included electron translational factors [25] used to modify the molecular eigenfunctions to remove asymptotic couplings between atomic states. Hence, we have limited our QMOCC collisions to the energy region of $E \leq 5$ keV/u.

B. TC-AOCC method for nonradiative charge transfer

The TC-AOCC equations are obtained by expanding the total electron wave function Ψ in terms of bound atomic orbitals of the two atomic centers multiplied by plane-wave electron translational factors (ϕ^A, ϕ^B),

$$\Psi(\vec{r}, t) = \sum_i a_i(t) \phi_i^A(\vec{r}, t) + \sum_j b_j(t) \phi_j^B(\vec{r}, t), \quad (8)$$

and by inserting this expansion into the time-dependent Schrödinger equation to generate the coupled equations for the state amplitudes [26]. In the present calculations, the straight-line approximation is adopted for the relative nuclear motion. The frozen core approximations for the Na^+ and Rb^+ ions are employed. The interaction of the active electron with the ionic cores for Na^+ and Rb^+ can be expressed as [2]

$$V_{\text{Na}^+}(r) = -\frac{1}{r} - \frac{1}{r}(10 + 17.9635r)e^{-3.5927r}, \quad (9)$$

$$V_{\text{Rb}^+}(r) = -\frac{1}{r} - \frac{1}{r}(36 - 1.975r)e^{-2.34113r}. \quad (10)$$

The resulting first-order coupled equations for the amplitude $a_i(t)$ and $b_j(t)$ are

$$i(\dot{A} + S\dot{B}) = HA + KB, \quad i(\dot{B} + S^\dagger\dot{A}) = \bar{K}A + \bar{H}B, \quad (11)$$

where A and B are the vectors of the amplitudes a_i and b_j , respectively. S is the overlap matrix (S^\dagger is its transposed form), H and \bar{H} are direct coupling matrices, and K and \bar{K} are

the electron exchange matrices. After solving the system of coupled equations (11), the cross section for $1 \rightarrow j$ electron-capture transitions is calculated as

$$\sigma_{cx,j} = 2\pi \int_0^\infty |b_j(+\infty)|^2 b db, \quad (12)$$

where b is the impact parameter. The sum of $\sigma_{cx,j}$ over j gives the corresponding total electron transfer cross section. In the present close-coupling calculations, we have a set of 32 atomic states with $l \leq 3$ in the Na center. Similarly, a set of 15 atomic states with $l \leq 2$ is used for the Rb target.

C. Fully quantum method for radiative charge transfer

In the present work, we use the fully quantum-mechanical approach [27,28] to calculate the radiative charge transfer. The radiative charge-transfer cross section can be given by

$$\sigma = \int_{\omega_{\min}}^{\omega_{\max}} \frac{d\sigma}{d\omega} d\omega, \quad (13)$$

with

$$\begin{aligned} \frac{d\sigma}{d\omega} = & \frac{8}{3} \left(\frac{\pi}{k_A} \right)^2 \frac{\omega^3}{c^3} \sum_J [JM_{J,J-1}^2(k_A, k_X) \\ & + (J+1)M_{J,J+1}^2(k_A, k_X)], \end{aligned} \quad (14)$$

where ω is the angular frequency of the emitted photon, c is the speed of light, the subscripts A and X denote the upper and the lower states, respectively, and

$$M_{J,J'}(k_A, k_X) \equiv \int_0^\infty dR f_J^A(k_A R) D(R) f_{J'}^X(k_X R), \quad (15)$$

where $D(R)$ is the dipole matrix element; k_A and k_X are the entrance and exit momenta, respectively,

$$\begin{aligned} k_A &= \sqrt{2\mu[E - V_A(\infty)]}, \\ k_X &= \sqrt{2\mu[E - V_X(\infty)] - \hbar\omega}, \end{aligned} \quad (16)$$

with E the relative collision energy in the center-of-mass frame. The partial wave $f_J^i(k_i R)$ ($i = X, A$) is the regular solution of the homogeneous radial equation

$$\left\{ \frac{d^2}{dR^2} - \frac{J(J+1)}{R^2} - 2\mu[V_i(R) - V_i(\infty)] + k_i^2 \right\} f_J^i(k_i R) = 0, \quad (17)$$

and is normalized asymptotically according to

$$f_J^i(k_i R) = \sqrt{\frac{2\mu}{\pi k_i}} \sin \left(k_i R - \frac{J\pi}{2} + \delta_J^i \right). \quad (18)$$

where δ_J^i ($i = X, A$) is the phase shift.

D. Optical-potential and semiclassical methods for radiative decay

The optical-potential method [27,29] is adopted to obtain the total cross sections for radiative decay, including both the radiative charge transfer and the radiative association. During the ion-atom collisions, the transition probability is represented by the imaginary part of a complex optical potential. The scattering wave $F_A(\vec{R})$, where R is the

internuclear distance and the subscript A denotes the initial upper molecular state ($A\ ^2\Sigma^+$), is obtained by solving the Schrödinger equation,

$$\left[-\frac{1}{2\mu}\nabla_R^2 + V_A(R) - E\right]F_A(\vec{R}) = \frac{i}{2}A(R)F_A(\vec{R}), \quad (19)$$

where E is the collision energy in the entrance channel, μ is the reduced mass, and $A(R)$ is the transition probability for the radiative transition given by

$$A(R) = \frac{4}{3}D^2(R)\frac{|V_A(R) - V_X(R)|^3}{c^3}, \quad (20)$$

where $V_A(R)$ and $V_X(R)$ are the adiabatic potential energy for the upper $A\ ^2\Sigma^+$ and the lower $X\ ^2\Sigma^+$ states, respectively. $D(R)$ is the transition dipole matrix element between the $A\ ^2\Sigma^+$ and $X\ ^2\Sigma^+$ states.

The cross section for collision-induced radiative decay can be written as

$$\sigma(E) = \frac{\pi}{k_A^2} \sum_J (2J+1)[1 - \exp(-4\eta_J)], \quad (21)$$

where η_J is the imaginary part of the phase shift for the J th partial wave of the radial Schrödinger equation which is given in the distorted-wave approximation by

$$\eta_J = \frac{\pi}{2} \int_0^\infty dR |f_J^A(k_A R)| A(R). \quad (22)$$

In order to extend our radiative-decay calculations to higher energies, replacing the summation in Eq. (21) and applying the JWKB approximation, one obtains the expression for the semiclassical cross section

$$\sigma(E) = 2\pi\sqrt{\frac{2\mu}{E}} \int p dp \int_{R_A^{\text{ctp}}}^\infty dR \frac{A(R)}{\sqrt{1 - V_A(R)/E - p^2/R^2}}, \quad (23)$$

where p is the impact parameter and R_A^{ctp} is the classical turning point in the incoming channel [27]. For large energies ($E \geq V_A$), the double integral is nearly energy independent, and therefore $\sigma(E)$ varies as $E^{-1/2}$. The difference between the total radiative-decay and the radiative charge-transfer cross section is the cross section for radiative association.

IV. RESULTS AND DISCUSSION

A. Nonradiative charge transfer

The QMOCC and AOCC methods have been applied to investigate the nonradiative charge-transfer collisions of Na⁺ with ⁸⁷Rb atoms. The total and state-resolved cross sections are obtained for the energy range of 10⁻⁴–100 keV/u. As shown in Fig. 5, the total nonradiative charge-transfer cross sections obtained are compared with the results of the AOCC method by Lee *et al.* [2]. In the overlapping energy region of 0.08–5 keV/u, there is generally good agreement between the present QMOCC and AOCC results and the AOCC calculations of Lee *et al.* [2]. In the low-energy region for $E < 1$ keV/u, the slow decrease of the charge-transfer cross section results from the relatively strong $2\ ^2\Sigma^+ - 1\ ^2\Pi$ rotational coupling of this collision system, as discussed in Sec. II.

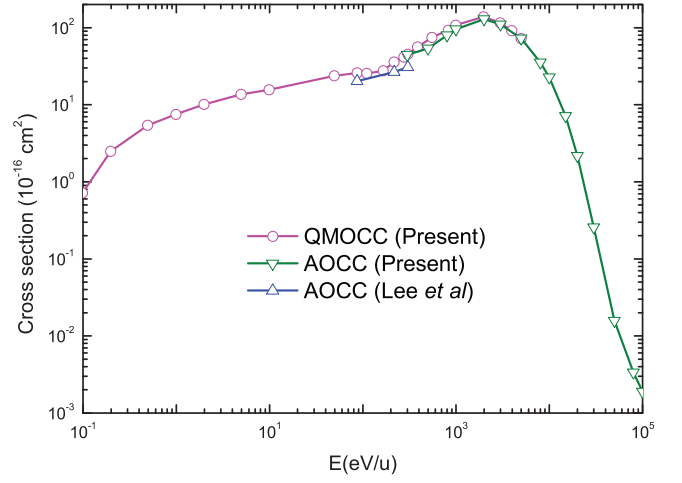


FIG. 5. (Color online) Total nonradiative charge-transfer cross sections for the Na⁺ + ⁸⁷Rb collisions. Shown are the present QMOCC results (solid line with open circles); present AOCC results (solid line with open downward triangles); AOCC results of Lee *et al.* [2] (solid line with open upward triangles).

In Fig. 6, the state-resolved cross sections for electron capture to the Na(3s) and Na(3p) states are presented and compared with the AOCC results of Lee *et al.* [2]. The present QMOCC and AOCC calculations to the Na(3p) state are in good agreement with the results obtained by Lee *et al.* [2] in the overlapping energy region of 0.08–5 keV/u. The present AOCC calculation to the Na(3s) state and the AOCC result by Lee *et al.* [2] are in good agreement at the energy of 0.3 keV/u. The QMOCC calculations to the Na(3s) state exceed the present AOCC results for energies above 0.3 keV/u. This difference is probably due to the fact that we have treated the potentials and couplings for $R < 1.5$ a.u. by extrapolation; they are not very accurate for the QMOCC calculations in the relatively high-energy region. Therefore, different and reliable

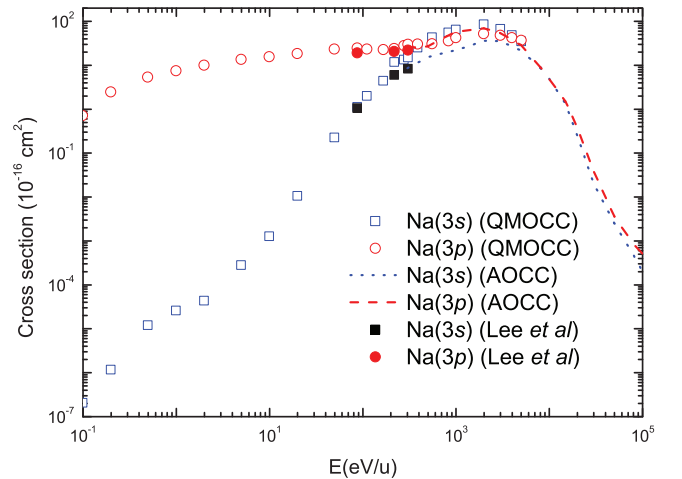


FIG. 6. (Color online) State-resolved nonradiative charge-transfer cross sections for the Na⁺ + ⁸⁷Rb collisions. Shown are present QMOCC results: 3s (open squares) and 3p (open circles); present AOCC results: 3s (dotted line) and 3p (dashed line); AOCC results of Lee *et al.* [2]: 3s (solid squares) and 3p (solid circles).

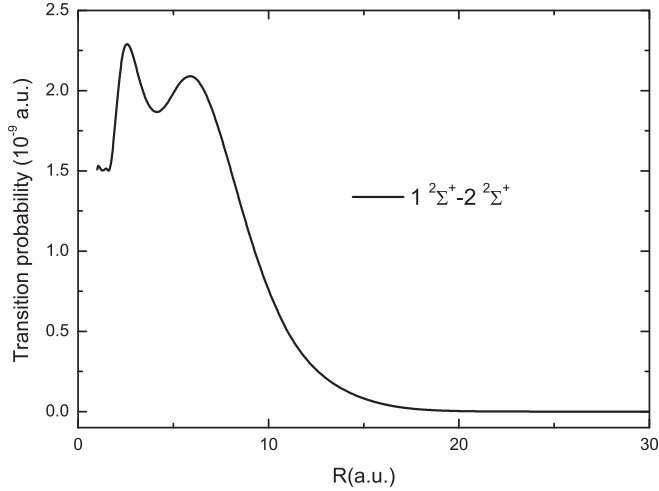


FIG. 7. Transition probability between $1\ ^2\Sigma^+$ and $2\ ^2\Sigma^+$ states as a function of internuclear distance.

experimental measurements and theoretical calculations are required to verify these results for this energy region.

B. Radiative decay, radiative charge transfer, and radiative association

In the present calculation, the upper A and the lower X states in Eqs. (14)–(23) correspond to the $2\ ^2\Sigma^+$ and the $1\ ^2\Sigma^+$ states, respectively. In this case, one only need consider the radiative processes from the initial channel of $2\ ^2\Sigma^+$ state to the lower $1\ ^2\Sigma^+$ state, which is dominated by the long-range polarization interaction. In the radiative calculation, the values of R_{\max} for matching the boundary conditions are increased from 500 to 2000 a.u. for collision energies varying from 0.2 to 10^{-18} eV/u, respectively. Beyond $R = 50$ a.u., the potentials of the $1\ ^2\Sigma^+$ and $2\ ^2\Sigma^+$ states are described by the long-range form

$$V_L(R) = -\frac{1}{2} \left[\frac{C_4}{R^4} + \frac{C_6}{R^6} + \frac{C_8}{R^8} \right], \quad (24)$$

where C_4 , C_6 , and C_8 are the dipole, quadrupole, and octopole polarizabilities of Na(3s) and Rb(5s) atom, respectively [30]. Based on the obtained potentials, the transition probability $A(R)$ is computed by using Eq. (20), and the result is shown in Fig. 7. There are two peaks near R of 2.60 and 5.90 a.u., respectively. The transition probability approaches zero as the internuclear distance increases beyond 15 a.u.

Using the optical-potential method, the radiative-decay (including the radiative charge-transfer and radiative-association) cross sections are calculated for energies from 10^{-18} to 5×10^{-3} eV/u, as shown in Fig. 8. For higher energies, the computational cost increases rapidly and a semiclassical calculation has been performed by using Eq. (23) for collision energies of 5×10^{-4} –0.2 eV/u. In the overlapping energy range of 5×10^{-4} – 5×10^{-3} eV/u, except for the shape resonance behavior, the semiclassical cross sections are in good agreement with the optical-potential results. The resonant structures, appearing in the energy region of 10^{-9} – 10^{-3} eV/u, are attributed to the presence of quasibound or virtual rotational-vibrational levels in the entrance channel. Apart from the resonance structures, the cross sections increase

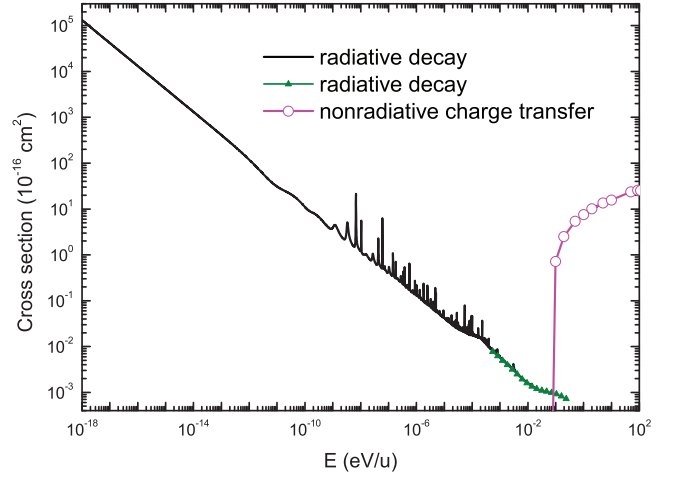


FIG. 8. (Color online) Comparison of the radiative-decay and nonradiative charge-transfer cross sections for $\text{Na}^+ + {}^{87}\text{Rb}$ collisions. Radiative-decay cross sections are obtained by the optical-potential method (solid line) and the semiclassical method (solid line with solid upward triangles), respectively, and nonradiative charge-transfer cross sections (solid line with open circles) are obtained by QMOCC method.

monotonically as the collision energies decrease. Most interestingly, the radiative-decay cross sections are well described by the classical $E^{-1/2}$ Langevin cross-section behavior [31] for collision energies from 10^{-18} to 10^{-2} eV/u in the asymmetric $\text{Na}^+ + \text{Rb}$ collisions.

For the convenience of comparison, the nonradiative charge-transfer results are also displayed in Fig. 8. For energy less than 0.1 eV/u, the radiative-decay processes are dominant and the nonradiative charge-transfer processes are negligible, where the electronic transitions are driven through the weak avoided crossing between the $1\ ^2\Sigma^+$ and $2\ ^2\Sigma^+$ states at an internuclear distance of $R = 11.50$ a.u. The large radiative-decay cross section provides a good way for ion cooling through collisions with cold neutral gas at extremely low energy. As the collision energy increases, the nonradiative charge-transfer cross sections increase steeply and become dominant for energies larger than 0.2 eV/u, where the electronic transitions occur mainly through the rotational coupling between the $2\ ^2\Sigma^+$ and $1\ ^2\Pi$ states.

In Fig. 9, the radiative charge-transfer cross sections are presented along with the radiative-decay cross sections and the radiative-association cross sections for the energy range of 10^{-18} – 3×10^{-3} eV/u. In the present calculations, the radiative charge-transfer cross sections are calculated from the fully quantum-mechanical approach using Eq. (13) and the radiative-association cross sections are obtained by subtracting the radiative charge-transfer part from the radiative-decay cross sections. It can be found that the radiative-association cross sections are about one order of magnitude larger than the radiative charge-transfer results and the radiative association dominates the radiative-decay processes. For the NaRb^+ system, a deep well (~ 0.531 eV) exists for the $1\ ^2\Sigma^+$ state at small internuclear distance and more quasibound vibrational levels can be formed. As the collision energy increases, the difference between the radiative-association

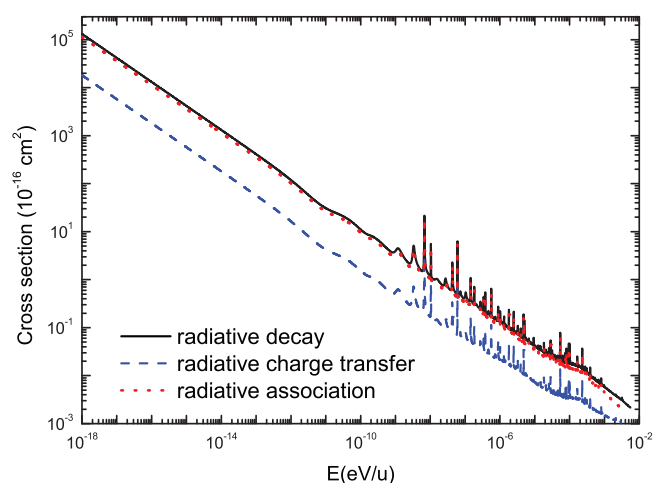


FIG. 9. (Color online) Comparison of the radiative charge-transfer (dashed line), radiative-decay (solid line), and radiative-association (dotted line) cross sections in the Na⁺ + ⁸⁷Rb collisions for the 2 ²Σ⁺ - 1 ²Σ⁺ transition.

and charge-transfer cross sections decreases quickly. With increasing collision energy, the effective angular momentum quantum numbers increase and the well in the effective potentials $V_j^{\text{eff}}(R) = V(R) + J(J+1)/2\mu R^2$ of the 1 ²Σ⁺ state will disappear at a relatively large value of J , causing the radiative-association cross sections to decrease quickly.

V. CONCLUSION

The nonradiative charge-transfer processes in Na⁺ + Rb(5s) collisions have been investigated by using the QMOCC and TC-AOCC methods for the energy range of

10⁻⁴ eV/u–5 keV/u and 0.3–100 keV/u, respectively. Good agreement has been obtained between the two calculations for the total and the dominant-channel capture cross sections in the overlapping energy range. The radiative-decay process is investigated by using the optical-potential and semiclassical methods in the collision energy range of 10⁻¹⁸–5 × 10⁻³ eV/u and 5 × 10⁻⁴–0.2 eV/u, respectively, and the two calculations join each other smoothly at ~10⁻³ eV/u. The radiative charge-transfer cross sections are calculated by using the fully quantum method in the energy range of 10⁻¹⁸–3 × 10⁻³ eV/u and the radiative-association results are obtained by subtracting the radiative charge-transfer part from the radiative-decay cross sections. It has been found that the nonradiative charge-transfer process dominates at energies above 0.2 eV/u, and the radiative process becomes dominant for energies below 0.1 eV/u. At the very low collision energies of 10⁻¹⁸–10⁻³ eV/u, the radiative-association process is more important than the radiative charge-transfer process. The radiative cross sections are very large, behaving as $E^{-1/2}$ and they vary approximately as the Langevin cross-section formula for a polarization potential for incident energy less than 10⁻² eV/u.

ACKNOWLEDGMENTS

This work was supported by the National Basic Research program of China under Grant No. 2013CB922200, the Foundation for the Development of Science and Technology of Chinese Academy of Engineering Physics under Grants No. 2012B0102015 and No. 2013A0102005, the National Science Foundation of China under Grants No. 10979007, No. 11025417, No. 11179041, and No. 11204017, and the Defense Industrial Technology Development Program under Grant No. b1520110011.

- [1] X. Flechard, H. Nguyen, R. Bredy, S. R. Lundeen, M. Stauffer, H. A. Camp, C. W. Fehrenbach, and B. D. DePaola, *Phys. Rev. Lett.* **91**, 243005 (2003).
- [2] T. G. Lee, H. Nguyen, X. Fléchar, B. D. DePaola, and C. D. Lin, *Phys. Rev. A* **66**, 042701 (2002).
- [3] J. Blicke, X. Fléchar, A. Cassimi, H. Gilles, S. Girard, and D. Hennecart, *Rev. Sci. Instrum.* **79**, 103102 (2008).
- [4] P. L. Gould, P. D. Lett, P. S. Julienne, W. D. Phillips, H. R. Thorsheim, and J. Weiner, *Phys. Rev. Lett.* **60**, 788 (1988).
- [5] C. D. Lin, T. Lee, and T. Y. Shi, *Nucl. Phys. Rev.* **19**, 140 (2002).
- [6] A. Rakshit and B. Deb, *Phys. Rev. A* **83**, 022703 (2011).
- [7] E. R. Hudson, *Phys. Rev. A* **79**, 032716 (2009).
- [8] R. Côté and A. Dalgarno, *Phys. Rev. A* **62**, 012709 (2000).
- [9] P. Zhang, A. Dalgarno, and R. Côté, *Phys. Rev. A* **80**, 030703(R) (2009).
- [10] H. A. Schuessler, C. H. Holder, Jr., and C.-S. O, *Phys. Rev. A* **28**, 1817 (1983).
- [11] O. Hadjar, D. Ascenzi, D. Bassi, P. Franceschi, M. Sabidò, and P. Tosi, *Chem. Phys. Lett.* **400**, 476 (2004).
- [12] R. J. Buenker and R. A. Phillips, *J. Mol. Struct.: THEOCHEM* **123**, 291 (1985).
- [13] S. Krebs and R. J. Buenker, *J. Chem. Phys.* **103**, 5613 (1995).
- [14] L. F. Pacios and P. A. Christiansen, *J. Phys. Chem.* **82**, 2664 (1985).
- [15] L. A. LaJohn, P. A. Christiansen, R. B. Ross, T. Atashroo, and W. C. Ermler, *J. Chem. Phys.* **87**, 2812 (1987).
- [16] G. Hirsch, P. J. Bruna, R. J. Buenker, and S. D. Peyerimhoff, *Chem. Phys.* **45**, 335 (1980).
- [17] Y. Ralchenko, A. E. Kramida, and J. Reader, NIST ASD Team, *NIST Atomic Spectra Database* (version 4.0.1) (2010). Available at <http://physics.nist.gov/asd>.
- [18] A. Valance, *J. Chem. Phys.* **69**, 355 (1978).
- [19] L. Bellomonte, P. Cavaliere, and G. Ferrante, *J. Chem. Phys.* **61**, 3225 (1974).
- [20] L. L. Yan, Y. Z. Qu, C. H. Liu, J. G. Wang, and R. J. Buenker, *J. Chem. Phys.* **136**, 124304 (2012).
- [21] B. Zygelman and A. Dalgarno, *Phys. Rev. A* **33**, 3853 (1986).
- [22] M. Kimura and N. F. Lane, *Adv. At. Mol. Phys.* **26**, 79 (1989).
- [23] B. R. Johnson, *J. Comput. Phys.* **13**, 445 (1973).
- [24] T. G. Heil, S. E. Butler, and A. Dalgarno, *Phys. Rev. A* **23**, 1100 (1981).
- [25] L. F. Errea, L. Méndez, and A. Riera, *J. Phys. B.* **15**, 101 (1982).

- [26] W. Fritsch and C. D. Lin, [Phys. Rep. **202**, 1 \(1991\)](#).
- [27] B. Zygelman and A. Dalgarno, [Phys. Rev. A **38**, 1877 \(1988\)](#).
- [28] P. C. Stancil and B. Zygelman, [Astrophys. J. **472**, 102 \(1996\)](#).
- [29] L. B. Zhao, J. G. Wang, P. C. Stancil, J. P. Gu, H.-P. Liebermann, R. J. Buenker, and M. Kimura, [J. Phys. B **39**, 5151 \(2006\)](#).
- [30] M. Marinescu, H. R. Sadeghpour, and A. Dalgarno, [Phys. Rev. A **49**, 982 \(1994\)](#).
- [31] P. Langevin, *Ann. Chim. Phys.* **5**, 245 (1905).